

Subaru/MOIRCS Near-Infrared Imaging in the Proto-Cluster Region at $z = 3.1$

Yuka Katsuno UCHIMOTO,^{1,2,3} Ryuji SUZUKI,^{2,3} Chihiro TOKOKU,^{2,3} Takashi ICHIKAWA,³
Masahiro KONISHI,^{2,3} Tomohiro YOSHIKAWA,^{2,3} Koji OMATA,² Tetsuo NISHIMURA,²
Toru YAMADA^{2,3} Ichi TANAKA,^{2,3} Masaru KAJISAWA,⁴ Masayuki AKIYAMA,^{2,3}
Yuichi MATSUDA,⁵ Ryosuke YAMAUCHI,⁶ and Tomoki HAYASHINO⁶

¹*Institute of Astronomy, University of Tokyo, 2-21-1 Osawa, Mitaka, Tokyo, 181-0015*
uchimoto@ioa.s.u-tokyo.ac.jp

²*Subaru Telescope, National Astronomical Observatory of Japan,*
650 North A'ohoku Place, Hilo, HI 96720, USA

³*Astronomical Institute, Tohoku University, Aramaki, Aoba, Sendai 980-8578*

⁴*National Astronomical Observatory, 2-21-1 Osawa, Mitaka, Tokyo, 181-8588*

⁵*Department of Astronomy, Kyoto University, Kitashirakawa-Oiwake-cho, Sakyo-ku, Kyoto 606-8502*

⁶*Research Center for Neutrino Science, Graduate School of Science,*
Tohoku University, Aramaki, Aoba-ku, Sendai, Miyagi, 980-8578

(Received ; accepted)

Abstract

We present the results of deep near-infrared imaging observations of the $z = 3.1$ proto-cluster region in the SSA22a field taken by MOIRCS mounted on the Subaru Telescope. We observed a 21.7 arcmin^2 field to the depths of $J = 24.5$, $H = 24.3$, and $K = 23.9$ (5σ). We examine the distribution of the K -selected galaxies at $z \sim 3$ by using the simple color cut for distant red galaxies (DRGs) as well as the photometric-redshift selection technique. The marginal density excess of DRGs and the photo- z selected objects are found around the two most luminous Ly α blobs (LABs). We investigate the correlation between the K -selected objects and the LABs, and find that several galaxies with stellar mass $M_* = 10^9 - 10^{11} M_\odot$ exist in vicinity of LABs, especially around the two most luminous ones. We also find that 7 of the 8 LABs in the field have plausible K_s -band counterparts and the sum of the stellar mass possibly associated with LABs correlates with the luminosity and surface brightness of them, which implies that the origin of Ly α emission may be closely correlated with their stellar mass or their previous star formation phenomena.

Key words: galaxies: clusters: general — galaxies: evolution — galaxies: formation — infrared: galaxies — galaxies: high-redshift

1. Introduction

The formation history of galaxies has been extensively studied in terms of the evolution of their stellar mass (Papovich et al. 2001; Kajisawa & Yamada 2006; Verma et al. 2007; Caputi et al. 2006; Fontana et al. 2006; Arnouts et al. 2007). However, it is still poorly constrained how galaxies developed their stellar systems in the early universe at $z > 2$. While the observed stellar mass density of the galaxies shows significant and rapid growth along the time at $z > 1$, at least 10 % of the present-day stellar mass in the galaxies is observed at $z \sim 3$ (Caputi et al. 2006; Fontana et al. 2006; Arnouts et al. 2007), which seems also true for the massive galaxies with $M_* > 10^{11} M_\odot$ (Caputi et al. 2006).

Where and how were they formed? The biased galaxy formation models in a universe dominated by cold dark matter suggest that galaxy formation preferentially occurs in regions with relatively high density at the larger scale (Kauffmann et al. 1999; Cen & Ostriker 2000; Benson et al. 2001; Bower et al. 2006). Recent results based on optical wide-field imaging reveal that high-redshift

star-forming galaxies indeed show very strong clustering largely biased to the expected underlying mass distribution (e.g., Steidel et al. 1998; Adelberger et al. 1998; Ouchi et al. 2001, 2005), which is also true for near-infrared (NIR)-selected massive galaxies (Daddi et al. 2003; Grazian et al. 2006; Quadri et al. 2007a; Foucaud et al. 2007; Ichikawa et al. 2007).

At $z = 2 - 3$, individual large-scale high-density regions of the galaxies have also been discovered (Steidel et al. 1998; Francis et al. 2001; Hayashino et al. 2004). Many of these fields are, however, identified as an excess in the number density of rest-frame UV bright galaxies, such as Ly α emitters (LAEs), Lyman Break Galaxies (LBGs) or their analogues. The question is how much of the stellar mass has already formed and assembled in such high density region of star-forming galaxies at $z \gtrsim 2$. In other words, we would like to see whether the structure traced by the star formation activity is correlated (or anti-correlated) with the structure traced by the stellar mass.

In this paper, we present the results of J -, H - and K_s -band imaging of the $z = 3.1$ proto-cluster region in and around the SSA22 field (Steidel et al. 1998,

2000; Hayashino et al. 2004) using Multi-Object InfraRed Camera and Spectrograph (MOIRCS) (Ichikawa et al. 2006; Suzuki et al. 2007) equipped with the 8.2 m Subaru Telescope. The wide field of view of MOIRCS allowed us to observe such proto-cluster regions efficiently.

The proto-cluster was first discovered by Steidel et al. (1998) as the excess of LBGs. Later wider-field and deeper narrow-band observations revealed that the overdense region of LBGs is a part of a large-scale high density structure of LAEs, which is extended over ~ 60 Mpc in a co-moving scale (Hayashino et al. 2004; Matsuda et al. 2004). Matsuda et al. (2005) confirmed that the structure has a three-dimensional filamentary appearance. Matsuda et al. (2004) also identified 35 Ly α Blobs (LABs, extended, bright Ly α -emitting clouds), along this structure. The large nebulae typically have Ly α luminosity $> 10^{43}$ - 10^{44} ergs s $^{-1}$ and physical extent 30-150 kpc. The most luminous and extended LABs are the two giant nebulae first discovered by Steidel et al. (2000) (hereafter referred as LAB1 and LAB2, following Matsuda et al. 2004). Rather than studying the differences in their distribution from only the UV-selected galaxies, observing the star forming regions in NIR, the rest-frame optical wavelengths puts more weight in their stellar mass content, allowing us to study the mass and population of the stars associated with them. The nature of dusty star-forming objects in such high-density structure can also be examined by the NIR data.

The field observed with MOIRCS (hereafter referred as SSA22-M1) corresponds to the southern part of SSA22a (Steidel et al. 2000) and is located within the field observed by Matsuda et al. (2004). In SSA22-M1, there are 8 LABs (Matsuda et al. 2004), 16 LAEs (Hayashino et al. 2004), and 17 LBGs (Steidel et al. 1998; Steidel et al. 2003b), of which 11 are located at $z = 3.1$. The sample selection for LAEs is overlapped with that for LABs. While LAEs are selected by the aperture photometry of the detected sources (Hayashino et al. 2004), LABs are selected by their isophotal area on the narrow-band image reduced with the optimum sky subtraction (Matsuda et al. 2004). Some LABs are associated with LAEs if they have enough compact high-surface brightness cores. On the other hand, Hayashino et al. (2004) excluded the LAEs detected in LAB1 and LAB2 from their sample as they are clearly un-isolated parts of diffuse Ly α nebulae. Two of the 16 LAEs in SSA22-M1 are identified with LABs (LAB16 and LAB31, referred by Matsuda et al. 2004).

We describe the observation and the data analysis method in section 2. The number density and the sky distribution of distant red galaxies (DRGs, Franx et al. 2003), the result of photometric redshift analysis of the K -selected sources, and the photometric properties of LABs, LBGs, and LAEs are shown in section 3. In section 4 we discuss our results in terms of the mass assembly history in the proto-cluster. We use the cosmological parameter values $\Omega_M = 0.3$, $\Omega_\Lambda = 0.7$, and $H_0 = 70$ km s $^{-1}$ Mpc $^{-1}$ throughout this paper. All the magnitude values are in AB system (Oke & Gunn 1983; Fukugita et al. 1996) unless explicitly noted.

2. Observation and Data Analysis

J -, H -, and K_s -band images of the field centered at $(\alpha, \delta)_{2000} = (22^{\text{h}} 17^{\text{m}} 33.9^{\text{s}}, +00^{\circ}12'14'')$ were obtained using MOIRCS mounted on the Subaru Telescope on June 15, 16 and August 14 in 2005, and July 23 in 2006 (UT). MOIRCS uses two 2048×2048 HAWAII-2 arrays with the pixel scale $0''.117$ pixel $^{-1}$ and the field of view $4' \times 7'$.

The images are reduced in a standard manner with the MCSRED software packages (I. Tanaka et al. 2007, in preparation). For the K_s -band flat-fielding, we use on/off sets of domeflat images to avoid the thermal emission seen at the edge of the frames due to the foreground telescope structure. The median-sky for each frame is subtracted before the frames are stacked. If notable diffuse residual patterns remain after the median-sky subtraction, we further subtracted them by using the IRAF `imsurfit` command. We also subtract fringe patterns in each frame, if they appear, using the templates made from the images taken in the same run.

The total exposure times of the final images are 3,240 s, 3,600 s, 2,235 s for J , H , K_s , respectively. The effective area of the image is 21.7 arcmin 2 . The stellar image sizes are $0''.51$, $0''.47$, $0''.44$ for J , H , K_s , respectively. The limiting magnitudes are $J = 24.5$, $H = 24.3$, and $K = 23.9$ with 5σ in a $1.1''$ diameter aperture. We calibrated our NIR data to the UKIRT photometric system (Tokunaga et al. 2002). We convert between the Vega system to the AB system using $J = J_{\text{Vega}} + 0.95$, $H = H_{\text{Vega}} + 1.39$, $K = K_{\text{Vega}} + 1.85$. The summary of the observations is shown in Table 1.

For the detection and photometry, we use SExtractor (version 2.3) (Bertin & Arnouts 1996). The objects which have more than 16 connected pixels with 1.5σ above the background noise are selected. The $J - K$ color is measured in a $1''.1$ diameter aperture. The SExtractor MAG AUTO value is adopted as the K -band pseudo total magnitude. The K_s -band image is smoothed to be matched with the PSF in J -band for $J - K$ color measurement. The completeness in K_s -band is 95% at $K = 23.5$ and 50% at $K = 23.9$ for a point source.

We also use the optical $BVRi'z'$ bands data obtained by Hayashino et al. (2004) and U_n -band data (Steidel et al. 2003a)¹ to estimate the photometric redshift. As the FWHM of the U_n -band image is $1''.3$, we smoothed the $BVRi'z'JHK_s$ -band images to be matched and measured the colors in a $2''.6$ aperture. Narrowband (NB497; 4977 Å, FWHM 77 Å) images used in section 3.3 are taken in Matsuda et al. (2004).

We corrected our data for the Galactic extinction adopting the average value at the field, $E(B - V) = 0.08$ (Schlegel et al. 1998).

3. Results

In this section, we present the observed properties of the K -selected objects in SSA22-M1. Since we are studying

¹ <ftp://ftp.astro.caltech.edu/pub/ccs/lbgsurvey/>

Table 1. Summary of the NIR observations

Filter	Integration s	FWHM arcsec	Limiting Mag. mag *
J	3,240	0.51	24.5
H	3,600	0.47	24.3
K_s	2,235	0.44	23.9

* The 5σ limit for a point source in a $1.1''$ diameter aperture.

the galaxies at $z = 3.1$, we need to apply some photometric selections to suppress the contamination of foreground/background objects. While full photometric redshift analysis is useful, it may suffer from misidentification especially for K -band faint objects because the optical data used here may not be deep enough for them to achieve high photometric accuracy. Simple color-cut method such as selecting DRGs with $(J - K)_{\text{Vega}} > 2.3$ (Franx et al. 2003) works complementary, so that we can more completely pick-up objects possibly located at $z = 3.1$, if they exist. We therefore first investigate the distribution of DRGs and then that of the photometric redshift (photo- z) selected sources to compare with the UV-selected objects in the field.

3.1. The Selection and Number Density of DRGs

We first focus on the distribution of DRGs in our field. DRGs are supposed to be evolved, relatively massive galaxies ($M_* \sim 10^{10} - 10^{11} M_\odot$) at $2 \lesssim z \lesssim 4$ (Franx et al. 2003; Förster Schreiber et al. 2004; Reddy et al. 2005; Ichikawa et al. 2007) or dusty galaxies at $z \gtrsim 1$ (Webb et al. 2006; Conselice et al. 2007; Quadri et al. 2007b; Lane et al. 2007). In the analysis of the deep multicolor data obtained at GOODS-N, Kajisawa et al. (2006) found that 83% of the DRGs with $22 < K < 23.5$ have the photometric redshift $z > 2$, while more than a half of the DRGs with $K < 22$ have $z < 2$. Thus the faint DRGs are supposed to be dominated by the galaxies at high redshift. As Marchesini et al. (2007) suggested that the global stellar mass at $2 \lesssim z \lesssim 3.5$ appears to be dominated by DRGs, the number of DRGs might be a good indicator of massive galaxies at $z \gtrsim 2$. In fact, Labbé et al. (2005) showed that DRGs dominate the high mass end of the mass function at high redshift.

We use the same criteria as in Kajisawa et al. (2006), which corresponds to $(J - K)_{AB} > 1.4$ in our photometric system. The red $J - K$ color of DRGs is due to the Balmer or 4000\AA break of galaxies at $z \gtrsim 2$, or due to the dust extinction (Franx et al. 2003; Reddy et al. 2005; Förster Schreiber et al. 2004). The color $(J - K)_{AB} > 1.4$ corresponds to that of a galaxy at $z = 3.1$ with the stellar population age older than 200 Myr if no extinction and the solar metallicity are assumed (Bruzual & Charlot 2003). Förster Schreiber et al. (2004) reported the median age and stellar mass for DRGs with $K < 25.6$ in HDF-S are 1.7 Gyr and $M_* = 0.8 \times 10^{11} M_\odot$. The K -band selected DRGs are supposed to be relatively more massive, more evolved

objects than ultra-violet(UV)-selected galaxies like LBGs at the same epoch.

In Fig. 1, we show the K versus $J - K$ color-magnitude diagram of the K -selected objects. The objects with $J - K \lesssim 0$ are likely to be galactic stars. The color of the sequence coincides with that seen in the other field (Kajisawa et al. 2006), which suggests that our photometric calibration is robust. The 2σ limiting magnitude in J -band is indicated by the solid line in Fig. 1. The J -band image is deep enough to select DRGs down to $K = 24.1$. The distribution of the photometric redshifts for DRGs is shown in Fig. 2. The detailed photo- z analysis is described in section 3.2. We find that 62 % of DRGs are classified as $2 < z_{\text{photo}} < 4$.

The cumulative number of DRGs in our observed field is 28 and the surface density is 1.29 arcmin^{-2} at $K < 23.35$ (or $K_{\text{Vega}} < 21.5$), which is comparable with that in GOODS-N by Kajisawa et al. (2006), $1.36 \pm 0.26 \text{ arcmin}^{-2}$ to the same depth. Fig. 3 compares the differential number counts for DRGs in our observed field with those in GOODS-N. Our sample is dominated by DRGs with $22 < K < 23.5$, which implies most of them should be at high redshift. The completeness fraction and the 95% limit, $K = 23.5$, are also marked. We do not see any notable excess in the number counts in SSA22-M1 over the magnitude range.

We note that there are nine hyper extremely red objects (HEROs, Totani et al. 2001) with $(J - K)_{AB} > 2.1$ in SSA22-M1 at $K < 23.5$. The surface density of HEROs at $K < 23.5$ is $0.41 \pm 0.14 \text{ arcmin}^{-1}$ which is consistent with those in SDF, HDF-S, and GOODS-N within the error (Maihara et al. 2001; Saracco et al. 2004; Kajisawa et al. 2006).

The sky distribution of DRGs is shown in Fig. 5a, and LABs (Matsuda et al. 2004), LAEs (Hayashino et al. 2004), and LBGs (Steidel et al. 2003b) are plotted in Fig. 5c. We then investigated the spatial correlation between DRGs and other UV-selected objects in the field. Fig. 6a shows the mean surface number density of DRGs as a function of a distance from LABs, LAEs, and LBGs.

First, we note that the distribution of the DRGs is weakly correlated with the sample of LABs as well as LBGs. Since the LBGs are associated with 7 of 8 LABs, it is not surprising that the similar correlations with DRGs are seen for these two populations. We also plotted the profile from the two distinctive giant LABs, namely LAB1 and LAB2 and found that the DRG density shows the notable excess within 1.0 arcmin (1.9 Mpc at $z = 3.1$ in comoving scale) around them. In fact, the correlation between DRGs and LABs is found to be dominated by the two objects; if we remove them from the sample, the correlation seen in Fig. 6a diminishes significantly.

As mentioned in the beginning of this section, the redshift range of the DRG criteria is broad and there may be a chance projection of interlopers at intermediate redshift. We made a simple test to see if the density excess of DRGs around LAB1 and LAB2 is significant by evaluating the probability of finding similar excess around the eight randomly placed objects. We find the similar profile

in 592 among the 10000 trials, which gives the probability of $\approx 6\%$ in random distribution of LAB to the observed distributions DRGs. Thus the association of LAB1/LAB2 with DRGs is marginally significant ($\approx 2\sigma$). We investigate the closer look for the K -selected objects near the eight LABs in the field in section 3.3.

We also find that there is no significant positive correlation between DRGs and LAEs, while a hint of anti-correlation is seen at $\sim 6''$ separation. It should be noted that there is such anti-correlation among the massive DRGs and less massive LAEs.

3.2. Photometric Redshift of the K -selected Sources

Using the $U_nBVRI'z'JHK$ photometric data, we estimated the photometric redshift of all the K -selected sources using the HyperZ code (Bolzonella et al. 2000). The photometric redshift method performs the SED fitting with the redshift, spectral type, age, and dust extinction as free parameters. The best fit SED with its redshift is determined from the minimum χ^2 value. The template spectrum we use are derived from GALAXEV, which is the library of evolutionary stellar population synthesis models by Bruzual & Charlot (2003).

At $z \sim 3$, the uncertainty of the photo- z is typically $\Delta z \sim 0.5$ (Kajisawa & Yamada 2005; Reddy et al. 2005; Cirasuolo et al. 2007; Ichikawa et al. 2007). Fig. 4 shows the resulting photometric redshifts versus spectroscopic redshifts obtained by previous studies (Songaila et al. 1994; Cowie et al. 1996; Steidel et al. 1999; Steidel et al. 2003b; Abraham et al. 2004; Swinbank et al. 2004; Doherty et al. 2005). The relative errors $(z_{\text{photo}} - z_{\text{sp}})/(1 + z_{\text{sp}})$ in the redshift estimation are also shown in the bottom panel of the figure. The mean of relative errors for LBGs at $z \sim 3$ is -0.04 and the standard deviation is 0.08 (also see Table 3 in section 3.3). We therefore pick up the objects with $2.6 < z_{\text{phot}} < 3.6$ as the candidate galaxies at $z = 3.1$. We found 29 objects of which 9 are classified as DRGs and 6 are classified as LBGs.

Fig. 5b shows a sky plot of the K -selected sources, similar to Fig. 5a, but for those with $2.6 < z_{\text{phot}} < 3.6$ and $K < 23.5$. Four LBGs associated with LABs are not appeared since they are fainter than the limit in K -band. Cross correlation with LABs, LAEs, and LBGs for this sample is also shown in Fig. 6b. We find that the association between these K -selected sources at $z = 3.1 \pm 0.5$ and LABs, especially LAB1 and LAB2, seems significant. In contrast to DRGs, LABs excluding the two giant blobs show the association with the photo- z selected objects.

3.3. NIR Properties of the LABs

In this section, we investigate the NIR counterparts of the individual LABs. We find that the 88% of the LABs have plausible K_s -band candidates. K_s -band images in $25''$ -side box for 8 LABs are shown in Fig. 7 and Fig. 8. The green lines indicate the $NB497$ -band detection isophoto contours (Matsuda et al. 2004) and R -band sources are indicated with the red contours in the figures. LBGs in the field (Shapley et al. 2001; Steidel et al. 2003b)

are also marked. Of 11 LBGs at $z = 3.1$, 8 are associated with LABs. Of these, SSA22a-C11 (Steidel et al. 2003, associated with LAB1), M14 (LAB2), M4 (LAB7), C12 (LAB20), D3 (LAB30), and C4 (LAB31) are detected in the K_s -band, while C6 (LAB7) and C15 (LAB8) are not.

Photometric properties of K -selected objects around LABs are summarized in Table 2 and the evaluated photometric redshift and physical properties of the candidates of $z = 3.1$ galaxies are presented in Table 3. The stellar age, dust extinction, absolute magnitude, and stellar mass are derived from the SED fitting with GALAXEV (Bruzual & Charlot 2003) by assuming $z = 3.1$. We assume the Chabrier (2003) initial mass function (IMF), the Calzetti et al. (2000) extinction law, and a solar metallicity. The characteristic time scale is set at $\tau = 0, 1, 9$ Gyr. The star formation timescale, the color excess, and the age are varied as free parameters and the best fit SED is determined from the minimum reduced χ^2 value. The mass-to-light ratio $(M/L)_V$ and the total absolute magnitude (L_V) derived from GALAXEV are used for calculating the stellar mass. The errors of the stellar mass indicate the confidence level of 68 %.

For LAB1, there are five K -selected sources within the Ly α nebula. LAB1-#1 and #2 are likely to be foreground objects as their photometric redshifts are $z_{\text{phot}} < 1$. Steidel et al. (2000) already reported that there is the K_s -band counterpart candidate with extremely red $R - K$ color near the center of the Ly α nebula (LAB1-#3 in Fig. 7). We find that LAB1-#3 is classified as a DRG and LAB1-#3 and #4 have $2.6 < z_{\text{phot}} < 3.6$. While their spectroscopic redshifts are still unknown, it is very likely that #4 associates the LAB as it is located right at the hole of Ly α nebulae (the right panel in Fig. 7); it may be an object which absorbs the Ly α emission at the redshift (Matsuda et al. 2007). #3 and #4 are also detected in Spitzer IRAC images in 3.6 - $8.0 \mu\text{m}$ (Geach et al. 2007; T. Webb et al. 2007, in preparation). The K_s -band counterpart of SSA22a-C11 at $z = 3.109$ is also detected (#5).

For LAB2, four K -selected sources are found. LAB2-#1 is classified as a DRG and it can be the counterpart of SSA22a-M14 ($z = 3.091$) although it is located at $0''.9$ north from the R -band position as mentioned in Ohyama et al. (2003). Probably, we see a mature or dusty part of the object in the K_s -band image. LAB2-#2 is likely to be foreground objects as the photometric redshift is $z_{\text{phot}} < 1$. LAB2-#4 is also classified as a DRG with extremely red color, $R - K = 4.32$.

In LAB7, Steidel et al. (2003b) and Shapley et al. (2001) sampled two LBGs, SSA22a-M4 ($z = 3.093$) and C6 ($z = 3.092$), whereas they are separated as three objects in $BVRi'z'$ -band images of Hayashino et al. (2004). Ly α emission entirely covers the three objects. From the coordinate we may identify the north component of this lump as LBG SSA22a-M4, which is detected in our K_s -band image. On the other hand, other two components are not detected either in the J nor in the K_s -band image.

LAB8 is located at $15''$ north of LAB1 and may form one large object (Matsuda et al. 2004). There is a LBG SSA22a-C15 ($z = 3.094$), which is not detected in either

J nor in K_s -band.

LAB16 is not associated with a LBG. We find a counterpart candidate in K_s -band whose $R-K$ color is slightly redder than those of typical LBGs at $z = 3.1$. The photometric redshift of the object is $z_{\text{phot}} = 2.7$.

LAB20, 30, and 31 are associated with the LBGs SSA22a-C12 ($z = 3.118$), D3 ($z = 3.086$), and C4 ($z = 3.076$), respectively. The K_s -band counterparts are detected for all of them.

Of the 16 LAEs, only two are detected in K_s -band and they are both associated with the LABs (LAB16 and LAB31, see above). From the upper limit of their K -band flux, for the rest 14 LAEs, we estimate that their stellar masses are lower than $\sim 2 \times 10^9 M_{\odot}$, assuming the spectrum of very young (10^6 -yr old) objects.

4. Discussion

We here discuss whether massive and/or mature galaxies have already formed in the cluster or proto-cluster which was characterized by the overdensity of star-forming galaxies.

There is the evidence that at least some relatively massive young galaxies ($10^{10} \sim 10^{11} M_{\odot}$) have been formed in the proto-cluster. Fig. 6b shows that the K -selected photo- z sample exhibits an excess within a radius of 0.1-0.7 arcminutes from the LABs. This indeed suggests that LABs are related to the formation of massive galaxies (Matsuda et al. 2006). We also found that DRG density shows a notable excess around LAB1 and LAB2. How unique are LAB1 and LAB2 among the 35 LABs in the same structure? They are the largest and the most luminous in $\text{Ly}\alpha$ emission. Moreover, Matsuda et al. (2005) suggested that LAB1 and LAB2 are located at the intersection of the filamentary structure of LAEs. Our results support the picture that LAB1 and LAB2 sit near the center of the proto-cluster, where the growth of the galaxy structure occurs most preferentially and we are witnessing a stage where a significant amount of the stars is being formed in such regions.

We also investigated the stellar mass of the K -selected objects, which are expected to be associated with LABs, by assuming they are located at $z = 3.1$ as described in section 3.2. The result is also tabulated in Table 3. Although the uncertainty of the stellar mass derived from the SED fitting is large, it is shown that the stellar mass of the LAB counterparts ranges from $4 \times 10^9 M_{\odot}$ to $1 \times 10^{11} M_{\odot}$.

Fig. 9a shows the relation between $\text{Ly}\alpha$ luminosity and the integrated stellar mass of the K -selected objects which are associated with each LAB, i.e., the objects in Table 3. Surface brightness of $\text{Ly}\alpha$ vs. the stellar mass is also shown in Fig. 9b. These figures suggest that the more massive galaxies are seen in the brighter LABs which have the higher surface brightness in $\text{Ly}\alpha$. This result implies the origin of the $\text{Ly}\alpha$ emission of LABs may be related with their previous star-formation history.

Since the local or intermediate-redshift clusters are dominated by the passively-evolving old galaxies, it is worth constraining how many such passive galaxies

formed at the higher redshift exist, if any, in the proto-cluster. In Fig. 1 we plotted the expected color-magnitude relation for the model galaxies with $M_V = -17$ to $M_V = -22$ at $z = 0$ of the Coma metallicity-sequence model (Kodama & Arimoto 1997). It is clearly seen that few objects have color and magnitude for such passive galaxies formed at $z_F > 4$. This result seems to be consistent with that in Kodama et al. (2007), which reported that the bright end of the red sequence in proto-clusters around radio galaxies appeared at $z \sim 2$, whereas it was not seen at $z \sim 3$.

Steidel et al. (2000) reported that the volume density of LBGs at $z \sim 3.1$ in the SSA22a/b fields, with the comoving volume of $2.7 \times 10^3 \text{ Mpc}^3$ in total, was 6 times higher than the average. They also evaluated the overdensity of LAEs which are typically 2 mag fainter than the LBGs in UV continuum to $R = 25.5$ in the SSA22a field and found a similar value. Hayashino et al. (2004) revisited the issue by using the deeper and wider-area data of LAEs. They confirmed the overdensity of ~ 6 around SSA22a in 10^3 Mpc^3 and found the overdensity of ~ 3 even at the $\sim 10^5 \text{ Mpc}^3$ volume.

We try to constrain the overdensity of such population of galaxies in the proto-cluster from the observed surface number density of DRGs in SSA22-M1. To obtain the number density of DRGs in a general field at $z \sim 3$, we adopt the luminosity function with $\phi^* = 6.14 \times 10^{-4} \text{ Mpc}^{-3} \text{ mag}^{-1}$, $M^* = -22.63$, and $\alpha = -0.46$ for DRGs at $2.7 < z < 3.3$ (Marchesini et al. 2007). Our limiting K -band magnitude corresponds to $M_V = -20.8$ and the expected number density of DRGs above the luminosity is $5.9 \times 10^{-4} \text{ Mpc}^{-3}$. The volume of the proto-cluster sampled in SSA22-M1 ($6' \times 3.5' \approx 11 \text{ Mpc} \times 7 \text{ Mpc}$ in comoving scale) is $1.4 \times 10^3 \text{ Mpc}^3$ if we assume the redshift range of $z = 3.08 - 3.10$, which is similar to those studied for the excess density of LBGs or LAEs. Consequently, the expected average number of DRGs in the volume of SSA22-M1 with $\Delta z = 0.02$ is obtained to be ≈ 0.8 .

We found at least three DRGs in vicinity of the two most luminous LABs (Table 2). As a result of the number density of DRGs, it is shown that approximately 5 DRGs at the redshift provides the similar overdensity as seen for LBGs or LAEs (≈ 6 times the average). Although the discussion is limited by the large uncertainty due to the small number of the objects, an overdensity similar to those of LBGs/LAEs is allowed if the number of the foreground/background DRGs in the field is less than $\sim 80\%$ of that in GOODS-N (29.5 DRGs are expected).

5. Summary

We presented the results of our deep near-infrared imaging observations of the $z = 3.1$ proto-cluster in the SSA22a field taken by MOIRCS mounted on Subaru Telescope. We observed 21.7 arcmin^2 field to the depths of $J = 24.5$, $H = 24.3$ and $K = 23.9$ with 5σ . Our observed field covers the area where the surface number density of the LAEs is highest.

We investigated whether massive and/or mature galax-

ies have already formed in the proto-cluster which is characterized by the overdensity of star-forming galaxies. We examined the distribution of the K -selected galaxies by using the simple color cut for DRGs as well as the photo- z selection. The surface number density of DRGs with $(J-K)_{AB} > 1.4$ in the field was 1.3 arcmin^{-2} at $K < 23.4$. While it was not likely that the density of DRGs have the similar excess as seen for LBGs at the volume, we found significant evidence that more than a few galaxies with the stellar mass $M_* = 10^9 - 10^{11} M_\odot$, exist in vicinity of, or might be associated with, the LABs.

We also investigated all the K_s -band counterparts which have the consistent photometric redshift not only for the LABs but also for the other objects at $z = 3.1$ in the field. We found that 88% of the LABs have the plausible K_s -band candidates. The sum of the stellar mass of the galaxies possibly associated with LABs correlated with the luminosity and surface brightness of the LABs, which implied that the origin of Ly α emission must be closely related with the massive galaxy formation phenomena. The most luminous LABs, LAB1 and LAB2, had the K -selected counterparts with $M_* \sim 10^{11} M_\odot$. In addition, the marginal density excess of DRGs and the photo- z selected objects was found around the most luminous LABs, LAB1 and LAB2.

Our results suggest that LABs are related to the formation of massive galaxies and a certain amount of evolved galaxies with $M_* \sim 10^{11} M_\odot$ are being formed in the central part of the high density region of star-forming galaxies at $z = 3.1$. We are witnessing a stage when significant amount of the stars are being formed in the central part of the growing large-scale proto-cluster at $z = 3.1$.

We thank the staff of the Subaru Telescope for their assistance with the development and the observation of MOIRCS. This study is based on data collected at Subaru Telescope, which is operated by the National Astronomical Observatory of Japan. This research is supported in part by the Grant-in-Aid for Scientific Research 11554005 and 14340059 of the Ministry of Education, Science, Culture, and Sports in Japan. The Image Reduction and Analysis Facility (IRAF) used in this paper is distributed by the National Optical Astronomy Observatories, U.S.A., which are operated by the Association of Universities for Research in Astronomy, Inc., under cooperative agreement with the National Science Foundation.

References

- Abraham, R. G., et al. 2004, AJ, 127, 2455
 Arnouts, S., et al. 2007, A&A, submitted (astro-ph/0705.2438)
 Adelberger, K. L., Steidel, C. C., Giavalisco, M., Dickinson, M., Pettini, M., & Kellogg, M. 1998, ApJ, 505, 18
 Basu-Zych, A. & Scharf, C. 2004, ApJ, 615, L85
 Benson, A. J., Frenk, C. S., Baugh, C. M., Cole, S., & Lacey, C. G. 2001, MNRAS, 327, 1041
 Bertin, E., & Arnouts, S. 1996, A&AS, 117, 393
 Bolzonella, M., Miralles, J.-M., & Pelló, R. 2000, A&A, 363, 476
 Bower, R. G., Benson, A. J., Malbon, R., Helly, J. C., Frenk, C. S., Baugh, C. M., Cole, S., & Lacey, C. G. 2006, MNRAS, 370, 645
 Bruzual, G. & Charlot, S. 2003, MNRAS, 344, 1000
 Caputi, K. I., McLure, R. J., Dunlop, J. S., Cirasuolo, M., & Schael, A. M. 2006, MNRAS, 366, 609
 Cen, R. & Ostriker, J. P. 2000, ApJ, 538, 83
 Calzetti, D., Armus, L., Bohlin, R. C., Kinney, A. L., Koornneef, J., & Storchi-Bergmann, T. 2000, ApJ, 533, 682
 Cirasuolo, M., et al. 2007, MNRAS, 380, 585
 Cowie, Lennox L.; Songaila, Antoinette; Hu, Ester M.; Cohen, J. G. 1996, AJ, 112, 839
 Chabrier, G. 2003, ApJ, 586, L133
 Conselice, C. J., et al. 2007, ApJ, 660, L55
 Daddi, E., Röttgering, H. J. A., Labbé, I., Rudnick, G., Franx, M., Moorwood, A. F. M., Rix, H. W., van der Werf, P. P., & van Dokkum, P. G. 2003, ApJ, 588, 50
 Doherty, M., Bunker, A. J., Ellis, R. S., & McCarthy, P. J. 2005, MNRAS, 361, 525
 Fontana, A., et al. 2006, A&A, 459, 745
 Förster Schreiber, N. M., et al. 2004, ApJ, 616, 40
 Foucaud, S., et al. 2007, MNRAS, in press astro-ph/0606386
 Francis, P. J., et al. 2001, ApJ, 554, 1001
 Franx, M. et al. 2003, ApJ, 587, 79
 Fukugita, M., Ichikawa, T., Gunn, J. E., Doi, M., Shimasaku, K., Schneider, D. P. 1996, AJ, 111, 1748
 Geach, J. E., Smail, I., Chapman, S. C., Alexander, D. M., Blain, A. W., Stott, J. P., & Ivison, R. J. 2007, ApJ, 655, L9
 Grazian, A., et al. 2006, A&A, 453, 507
 Hayashino, T., et al. 2004, AJ, 128, 2073
 Ichikawa, T., et al. 2006, in Proc. of SPIE, Vol. 6269, 38
 Ichikawa, T., et al. 2007, PASJ, in press (astro-ph/0701820)
 Im, M., Yamada, T., Tanaka, I., & Kajisawa, M. 2002, ApJ, 578, L19
 Kajisawa, M. & Yamada, T. 2005, ApJ, 618, 91
 Kajisawa, M., & Yamada, T. 2006, ApJ, 650, 12
 Kajisawa, M., et al. 2006, PASJ, 58, 951
 Kauffmann, G., Colberg, J. M., Diaferio, A., & White, S. D. M. 1999, MNRAS, 307, 529
 Kodama, T., & Arimoto, N. 1997, 320, 41
 Kodama, T., Tanaka, I., Kajisawa, M., Kurk, J., Venemans, B., De Breuck, C., Vernet, J. l, & Lidman, C. 2007, MNRAS, 377, 1717
 Labbé, I. et al. 2005, ApJ, 624, L81
 Laird, E. S., Nandra, K., Hobbs, A., Steidel, C. C. 2006, MNRAS, 373, 217
 Lane, K. P., et al. 2007, MNRAS, 379, L25
 Maihara, T., et al. 2001, PASJ, 53, 25
 Marchesini, D., et al. 2007, ApJ, 656, 42
 Matsuda, Y., et al. 2004, AJ, 128, 569
 Matsuda, Y., et al. 2005, ApJ, 634, L125
 Matsuda, Y., Yamada, T., Hayashino, T., Yamauchi, R., & Nakamura, Y. 2006, ApJ, 640, L123
 Matsuda, Y., Iono, D., Ohta, K., Yamada, T., Kawabe, R., Hayashino, T., Peck, A. B., & Petitpas, G. R. 2007, ApJ, 667, 667
 Oke & Gunn 1983, ApJ, 277, 713
 Ohya, Y., Taniguchi, Y., Kawabata, K. S., Shioya, Y., Murayama, T., Nagao, T., Takata, T., Iye, M., Yoshida, M. 2003, ApJ, 591, L9
 Ouchi, M., et al. 2001, ApJ, 558, L83

- Ouchi, M., et al. 2005, ApJ, 635, L117
- Papovich, C., Dickinson, M., & Ferguson, H. C. 2001, ApJ, 559, 620
- Quadri, R. et al. 2007, ApJ, 654, 138
- Quadri, R. et al. 2007, AJ, 134, 1103
- Reddy, N. A., Erb, D. K., Steidel, C. C., Shapley, A. E., Adelberger, K. L., & Pettini, M. 2005, ApJ, 633, 748
- Saracco, P., et al. 2004, A&A, 420, 125
- Schlegel, D.J., Finkbeiner, D. P., & Davis, M. 1998, ApJ, 500, 525
- Shapley, A. E., Steidel, C. C., Adelberger, K. L., Dickinson, M., Giavalisco, M., & Pettini, M. 2001, ApJ, 562, 95
- Steidel, C. C., Adelberger, K. L., Dickinson, M., Giavalisco, M., Pettini, M., & Kellogg, M. 1998, ApJ, 492, 428
- Steidel, C. C., Adelberger, K. L., Giavalisco, M., Dickinson, M., & Pettini, M. 1999, ApJ, 519, 1
- Steidel, C. C., et al. 2000, 532, 170
- Steidel, C. C., Adelberger, K. L., Shapley, A. E., Pettini, M., Dickinson, M., & Giavalisco, M. 2003a, arXiv:astro-ph/0305378
- Steidel, C. C., Adelberger, K. L., Shapley, A. E., Pettini, M., Dickinson, M., & Giavalisco, M. 2003b, ApJ, 592, 728
- Songaila, A., Cowie, L. L., Hu, E. M., & Gardner, J. P. 1994, ApJS, 94, 461
- Suzuki, R., et al. 2007, submitted to PASJ
- Swinbank, A. M., Smail, Ian, Chapman, S. C., Blain, A. W., Ivison, R. J., & Keel, W. C. 2004, ApJ, 617, 64
- Tokunaga, A. T., Simons, D. A., & Vacca, W. D. 2002, PSAP, 114, 180
- Totani, T., Yoshii, Y., Iwamuro, F., Maihara, T., & Motohara, K. 2001, ApJ, 558, L87
- Verma, A., Lehnert, M. D., Förster Schreiber, N. M., Bremer, M. N., & Douglas, L. 2007, MNRAS, 377, 1024
- Webb, T. M. A., et al. 2006, ApJ, 636, L17

Table 2. The NIR photometric properties of K -selected objects in LABs

LAB No.	Object ID *	RA	Dec	K	$J - K$ ($1''.1\phi$)	$R - K$ ($2''.0\phi$)
LAB1	C11 (#5)	22:17:25.7	0:12:34.6	23.18 ± 0.16	1.23 ± 0.42	1.31 ± 0.56
	#1	22:17:26.1	0:12:46.7	22.23 ± 0.10	1.08 ± 0.28	4.08 ± 0.51
	#2	22:17:25.8	0:12:43.8	22.75 ± 0.13	0.33 ± 0.26	1.34 ± 0.39
	#3	22:17:26.0	0:12:36.4	23.07 ± 0.15	1.48 ± 0.45	2.77 ± 0.51
	#4	22:17:26.1	0:12:32.3	22.38 ± 0.11	1.31 ± 0.33	2.20 ± 0.30
LAB2	M14 [†] (#1)	22:17:39.1	0:13:30.6	23.30 ± 0.16	1.60 ± 0.47	2.60 ± 0.64
	#2	22:17:39.1	0:13:26.4	22.26 ± 0.10	0.55 ± 0.25	1.13 ± 0.30
	#3	22:17:38.9	0:13:24.0	19.98 ± 0.03	0.50 ± 0.07	1.85 ± 0.03
	#4	22:17:39.3	0:13:22.1	22.63 ± 0.11	1.95 ± 0.41	4.32 ± 0.80
LAB7	M4	22:17:41.0	0:11:27.8	23.78 ± 0.19	0.23 ± 0.34	0.90 ± 1.02
	C6	-	-	-	-	-
LAB8	C15	-	-	-	-	-
LAB16		22:17:24.9	0:11:17.5	23.29 ± 0.16	0.91 ± 0.36	1.78 ± 0.59
LAB20	C12	22:17:35.3	0:12:47.4	24.12 ± 0.23	0.70 ± 0.44	0.49 ± 1.12
LAB30	D3	22:17:32.5	0:11:32.9	22.88 ± 0.13	0.73 ± 0.31	1.08 ± 0.41
LAB31	C4	22:17:39.0	0:11:26.1	23.39 ± 0.16	1.14 ± 0.41	1.29 ± 0.73

* ID of LBGs is referred from Steidel et al. (2003a).

[†] The associated NIR object of M14 is located at $0''.9$ apart from the peak of the rest-frame UV source.**Table 3.** The photometric redshift and stellar mass of NIR counterparts

LAB	Object ID *	z_{spec} [†]	z_{photo}	Age [‡] (Gyr)	E(B-V) [‡] (mag)	Mv [‡] (mag)	Stellar Mass [‡] ($10^{10}M_{\odot}$)
LAB1	C11	3.109	2.83	1.80	0.08	-22.32	$2.5^{+2.4}_{-1.5}$
	#3	-	2.85	1.80	0.20	-22.59	$7.2^{+4.3}_{-2.5}$
	#4	-	2.61	1.61	0.18	-23.19	$10.9^{+4.8}_{-5.0}$
LAB2	M14 [§]	3.091	3.19	1.80	0.22	-22.64	$8.1^{+4.8}_{-6.9}$
	#4	-	2.61	0.20	0.40	-23.05	$10.5^{+32.6}_{-6.3}$
LAB7	M4	3.093	2.70	0.57	0.06	-21.75	$0.7^{+2.8}_{-0.7}$
LAB16	-	-	2.70	0.06	0.20	-22.50	$1.6^{+3.6}_{-1.2}$
LAB20	C12	3.118	2.85	0.57	0.00	-21.43	$0.4^{+1.1}_{-0.3}$
LAB30	D3	3.086	3.31	1.61	0.08	-22.74	$3.4^{+1.1}_{-2.1}$
LAB31	C4	3.076	3.19	1.80	0.00	-22.04	$2.0^{+1.5}_{-1.4}$

* ID of LBGs is referred from Steidel et al. (2003a).

[†] The redshifts of LBGs are referred from Steidel et al. (2003a).[‡] The redshifts are assumed to be $z = 3.1$ when the SEDs are calculated.[§] The associated NIR object of M14 is located at $0''.9$ apart from the peak of the rest-frame UV source.

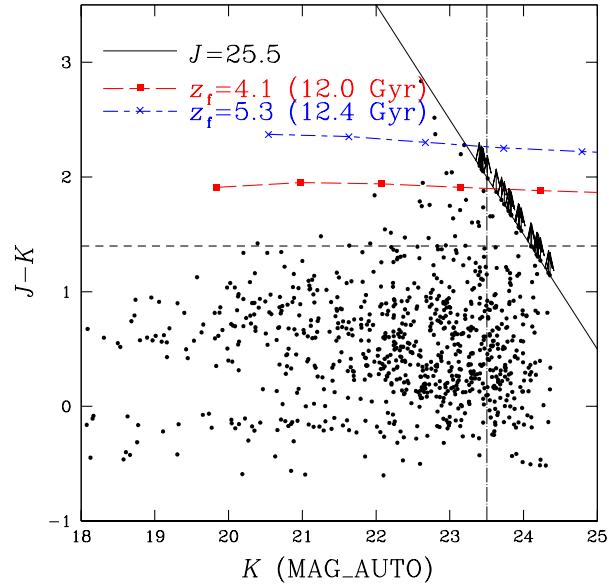


Fig. 1. K vs. $J-K$ color-magnitude diagram of the K -selected objects. The solid line indicates the detection limit of 2σ above the sky fluctuation in J -band. The vertical dot-dashed line shows the K -band completeness limit of 95 %. The horizontal dashed line shows $J-K = 1.4$. The expected color-magnitude relations of cluster galaxies calculated by Kodama & Arimoto (1997) for Coma cluster model with the formation redshift at $z_f = 4.1$ and $z_f = 5.3$ are plotted with the squares and the crosses, respectively. The points indicate the location of model galaxies with the rest-frame V -band luminosity from $M_V = -17$ to $M_V = -22$ at $z = 0$. The objects with $J-K \lesssim 0$ are expected to be galactic stars.

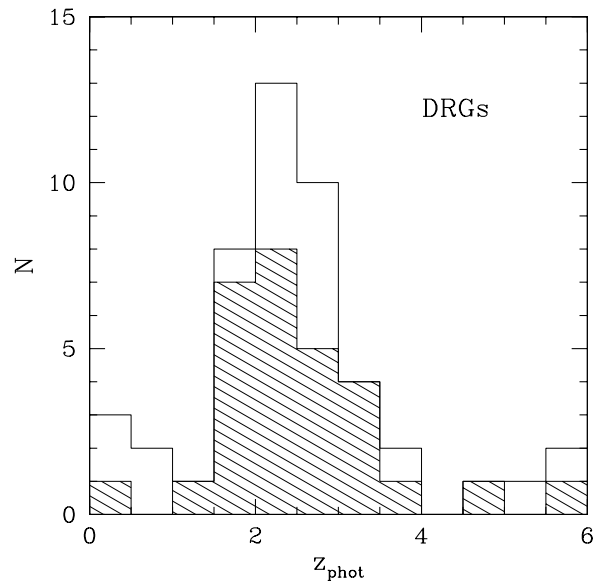


Fig. 2. Histogram of the estimated photometric redshift of DRGs. The hashed histogram is DRGs with $K < 23.5$.

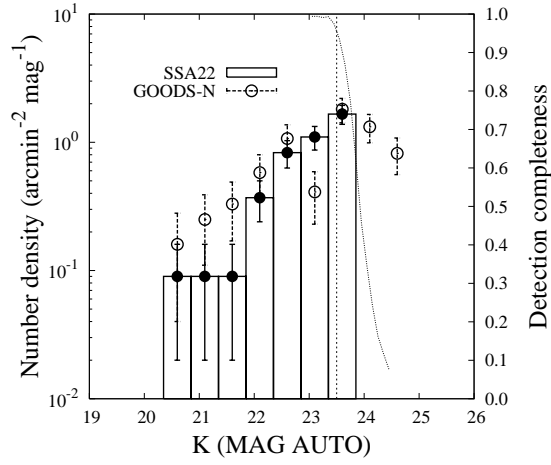


Fig. 3. Differential number counts for DRGs in our observed field (filled circles) in comparison with those for DRGs in the GOODS-N field (open circles) (Kajisawa et al. 2006). The vertical dotted line shows the K -band completeness limit of 95 %. The detection completeness in K -band is also shown with the smaller dotted line.

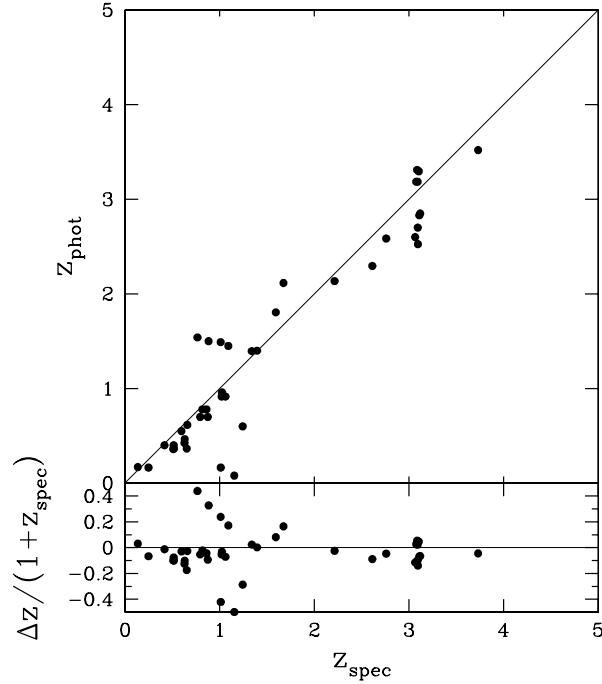


Fig. 4. Spectroscopic and photometric redshifts of galaxies for the K -selected objects in the SSA22-M1 field. The relative errors $(z_{\text{photo}} - z_{\text{sp}})/(1 + z_{\text{sp}})$ are indicated in the bottom panel.

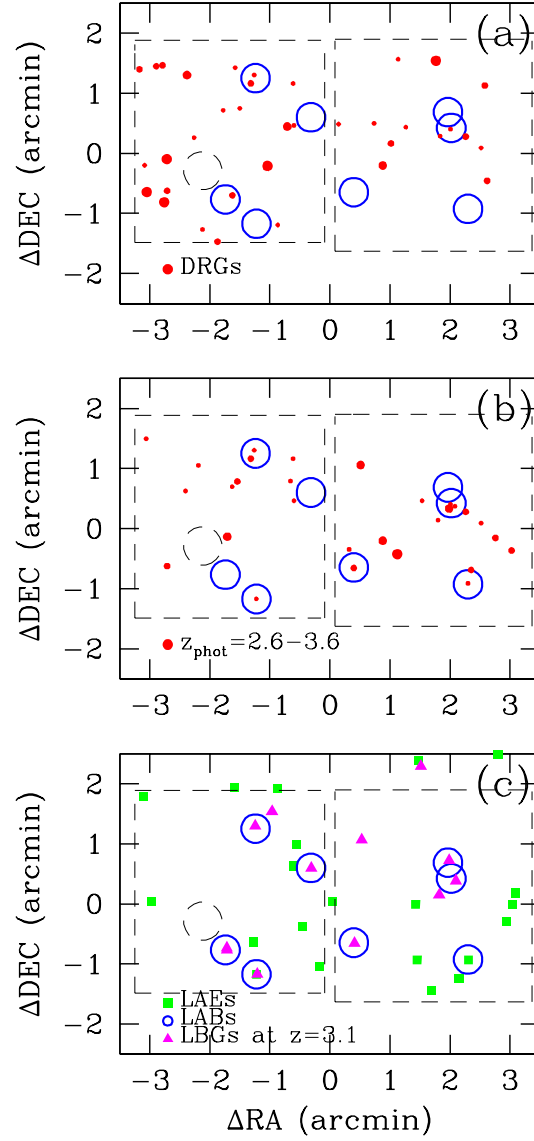


Fig. 5. (a) Sky distribution of DRGs and LABs. DRGs are indicated with filled circles (red). LABs are indicated with large open circles (blue). Dotted squares indicate the observed regions with MOIRCS. The dotted large circle at the east side is the region excluded from the analysis due to a bright star. (b) Sky distribution of $z_{\text{phot}} = 2.6 - 3.6$ objects with $K < 23.5$ and LABs. The objects are indicated with filled circles (red). (c) Sky distribution of LABs, LAEs and LBGs. LAEs (square, green) from Hayashino et al. (2004) and LABs (large open circle, blue) from Matsuda et al. (2004) are shown. LBGs at $z = 3.1$ from Steidel et al. (2003) are indicated with triangles (magenta).

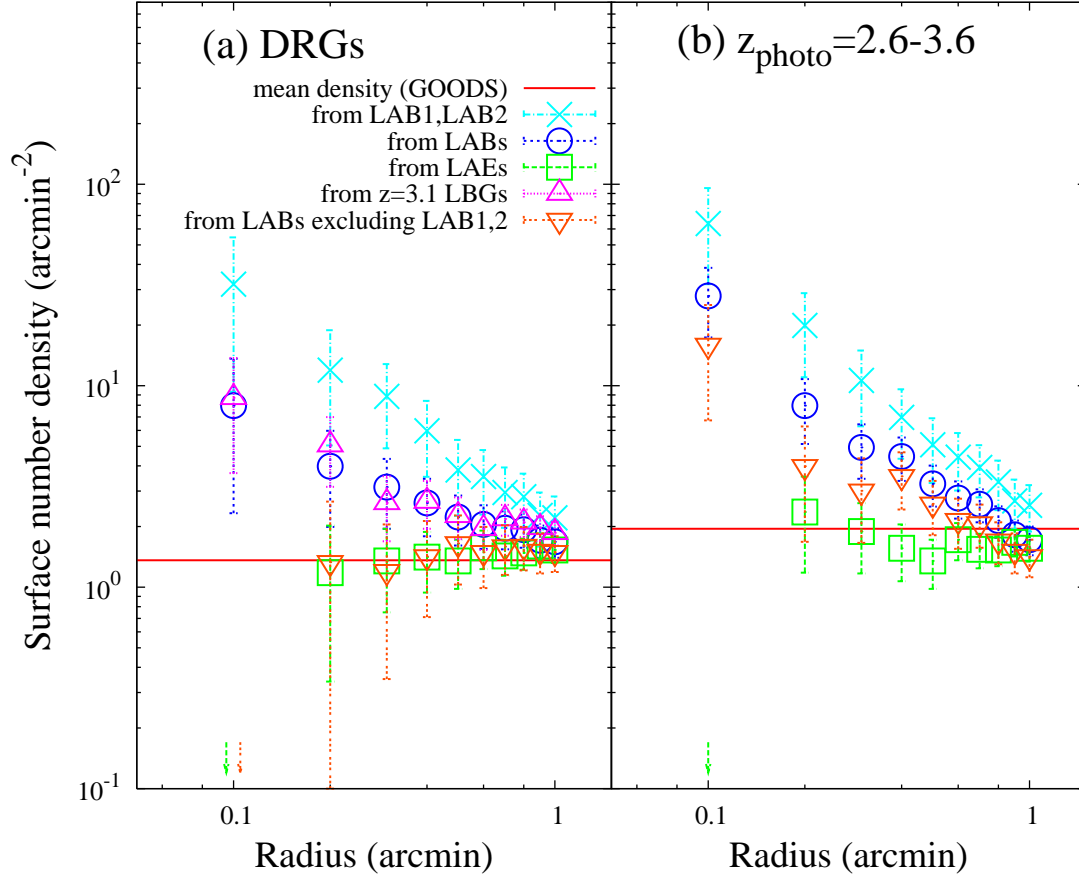


Fig. 6. (a) The mean surface number density of DRGs around optically selected galaxies. The horizontal axis is radial distance from LABs, LAEs or LBGs. The surface densities of DRGs from LAB1 and LAB2, LABs, LAEs, LBGs, and LABs excluding LAB1 and LAB2 are shown as crosses (cyan), open circles (blue), open squares (green), open triangles (magenta), and inverted triangles (orange), respectively. The mean density of DRGs in GOODS-N (Kajisawa et al. 2006) is also indicated with a solid line. The arrows indicate zero at $r = 0.1$ arcmin. (b) The mean surface number density of $z_{\text{phot}} = 2.6 - 3.6$ objects with $K < 23.5$ around optically selected galaxies. The mean density of $z_{\text{phot}} = 2.6 - 3.6$ objects in GOODS-N (Ichikawa et al. 2006) is also indicated with a solid line.

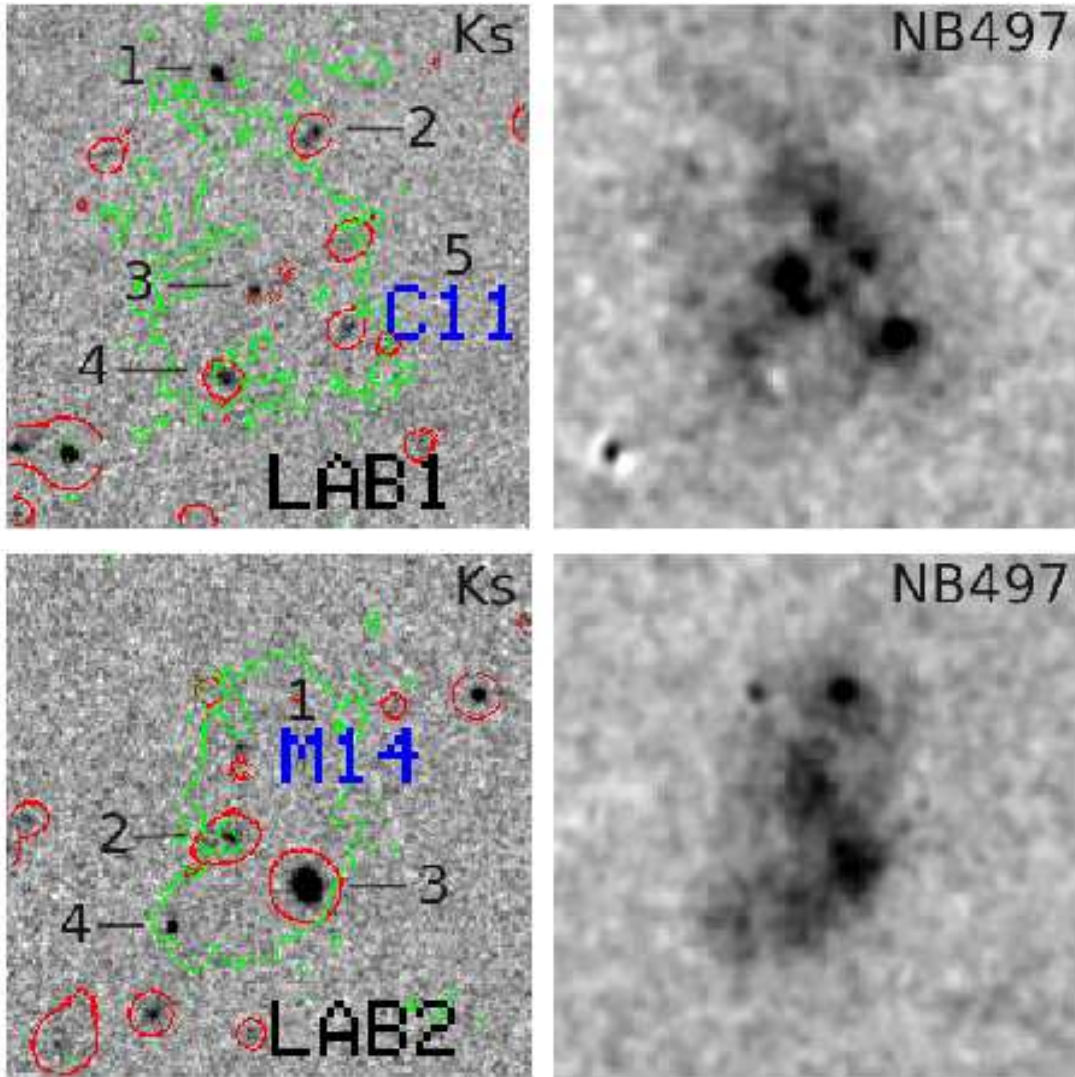


Fig. 7. K_s -band and narrowband (NB497; 4977 Å, FWHM 77 Å) images around LAB1 and LAB2 at $z = 3.1$ (Matsuda et al. 2004). The size of each panel is $25''$, which corresponds to ~ 190 kpc at $z = 3.1$. Each image is centered on a LAB from Matsuda et al. (2004). The green and red contours are the isophotal levels of NB497 and R -band images, respectively.

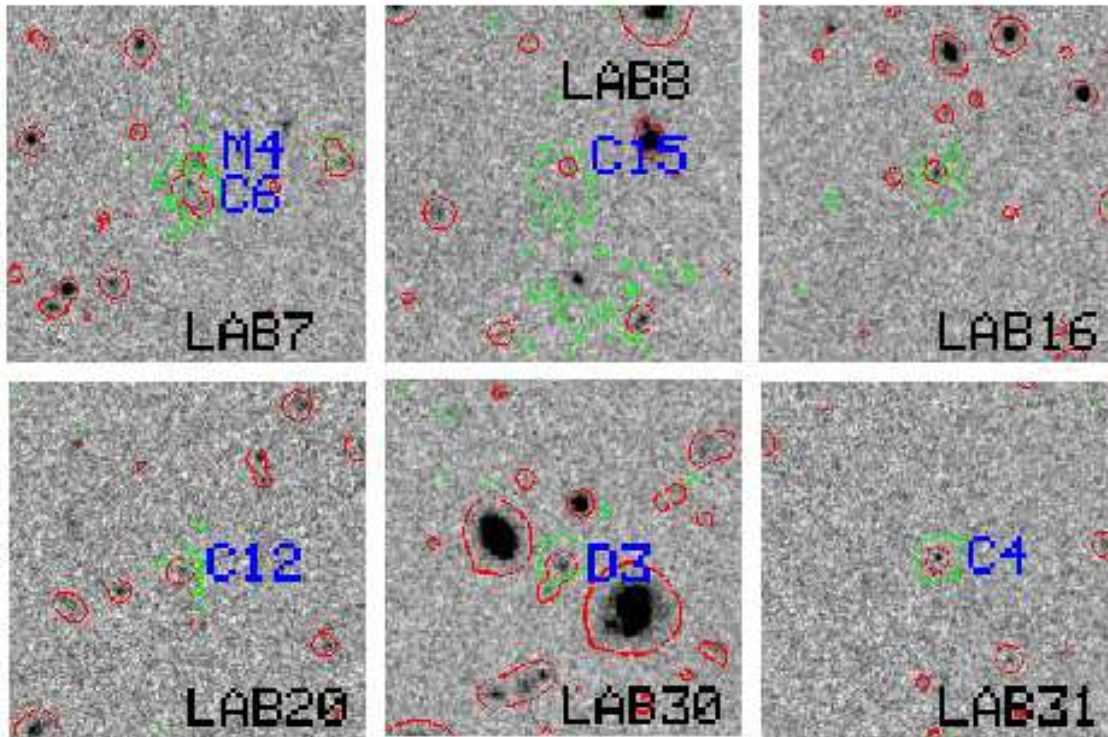


Fig. 8. K_s -band images around LABs at $z = 3.1$ (Matsuda et al. 2004). The size of each panel is $25''$, which corresponds to ~ 190 kpc at $z = 3.1$. Each image is centered on a LAB from Matsuda et al. (2004). The green and red contours are the isophotal levels of NB497 and R -band images, respectively.

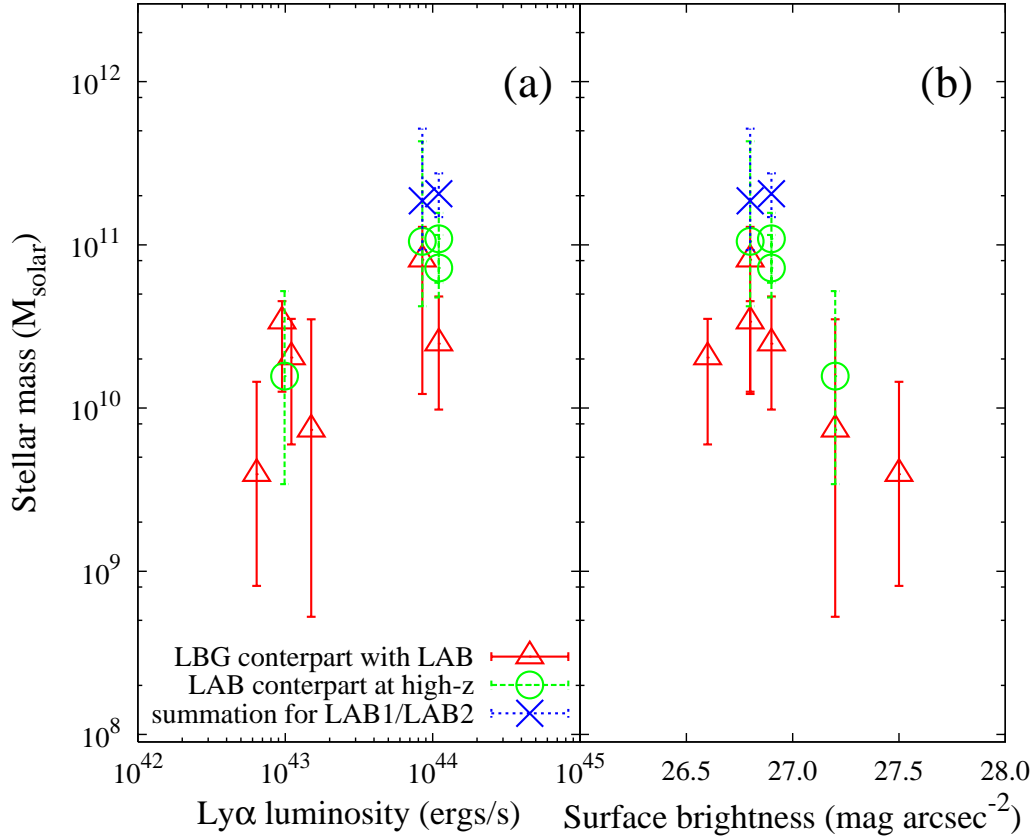


Fig. 9. (a) Ly α luminosity vs. the stellar mass of the NIR-counterpart candidates. (b) Surface brightness of Ly α vs. the stellar mass of the NIR-counterpart candidates (see text). The redshift of NIR objects is assumed to be $z = 3.1$. LBG counterparts associated with LABs are indicated with open triangles (red) and K -selected objects expected to be associated with LAB, but with no LBGs, are indicated with open circles (green). Since LAB1 and LAB2 include several NIR counterparts, the total stellar masses in each LAB are indicated with blue crosses.